Accessibility in Liquid Media: Cyclodehydration of Hexane-2,5-Diol for the Evaluation of Layered Catalysts

Moussa Zaarour, Ghinwa Fayad, Philippe Boullay, Guillaume Clet

Accessibility in liquid media: Cyclodehydration of hexane-2,5-diol for the evaluation of layered catalysts

*Moussa Zaarour, Ghinwa Fayad, Philippe Boullay and Guillaume Clet**

Dr. Moussa Zaarour, Dr. Ghinwa Fayad, Dr. Guillaume Clet
Normandie Univ, ENSICAEN, UNICAEN, CNRS, LCS, 14000 Caen, France

Dr. Philippe Boullay
Normandie Univ, ENSICAEN, UNICAEN, CNRS, CRISMAT, 14000 Caen, France

Keywords : layered materials, $HNbMoO_6$, intercalation, liquid-phase catalysis, Raman, hexane-2,5-diol, 2,5-dimethyltetrahydrofuran

Abstract

In order to establish layered materials as heterogeneous catalysts in the liquid phase, acidic layered materials are evaluated here through the conversion of hexane-2,5-diol used as a model reaction. Such polyoxygenate reactant is representative of some of the biomass components and the interactions of the reagent or furan product with the interlayers surface is a key to the understanding of these lamellar materials features. Layered $HNbMoO_6$ catalyst is particularly active and stable for the studied reaction compared to several zeolites and its high activity is obtained without any pre-activation step prior to reaction. The influence of temperature and water content in the reaction mixture are also studied for this catalyst. The importance of intercalation in the reaction process is specifically evaluated using Raman spectroscopy and powder X-ray diffraction (PXRD). On this layered catalyst, the reaction proceeds after intercalation of diol within the interlayer space followed by subsequent cyclodehydration giving rise to 2,5-dimethyltetrahydrofuran with high selectivity. Comparison with related layered materials such as $HNbWO_6$ or $H_2W_2O_7$ highlights a distinct behavior both in reactivity and intercalation and emphasizes the role of the accessibility to the active sites.

1. Introduction

Biomass conversion has been the focus of numerous studies recently. Using these compounds in various processes instead of petroleum-based compounds involves new constraints induced by oxygenated compounds and potentially large amounts of water. This replacement raises new concerns not only on the catalysts that can be used, heterogeneous catalysts in particular [1], but also on the relevant characterization methodologies and the mere evaluation of their catalytic activity. In this context, the development of a simple model reaction is desirable to assist the screening process of suitable catalyst formulations, similar to what was developed in many years for the conversion of petroleum-based compounds, very often for gas phase conversions. Conversely, liquid phase conversions might be more representative of biomass reactants. Among possible reactions, polyoxygenates such as diols could be used to model some of the reactions observed with sugars. The cyclodehydration of diols is an acid-catalyzed reaction [2] that gives rise to furanic compounds, a valuable class of chemicals. The protonation of one hydroxyl group allows the oxygen lone pair of the other amphoteric hydroxyl to attack the partially positively charged carbon, thus producing cyclic ether [3]. Additionally, a limited amount of by-products can be expected, which is desirable for a simpler test.

Converting polyoxygenate compounds such as 1,4-butanediol into furanic compounds was investigated by several researchers over various solid acid catalysts [2,4–7]. However, the conversion of larger chain alcohols, more representative of sugars, such as hexanediol is less addressed. Yamaguchi and co-workers [8] reported the intramolecular dehydration of chiral hexane-2,5-diol (2R,5R) or (2S, 5S) to cis-2,5-dimethyltetrahydrofuran using high-temperature liquid water (523 K) and high carbon dioxide pressure. Other groups reported the cyclodehydration of hexane-2,5-diol using either an enzyme (Lipase AK) and an intermediate transesterification step [9], a homogeneous acid catalyst such as sulfuric or phosphoric acids [10], or metal chlorides such as $PdCl_2$ or $AlCl_3$ [7]. The conversion of hexanediol is important because the two secondary hydroxyl groups of hexane-2,5-diol are separated by four carbon atoms; their

location permits the formation of 5-membered ring tetrahydrofuran derivative. On the other hand, the presence of non-terminal alcohol promotes the formation of alkene derivatives, dehydration by-products [3,6,7]. Hence, this reaction may constitute a valuable test for both the activity and the selectivity of the catalyst. Interestingly, hexane-2,5-diol cyclodehydration is also considered as the last step in the conversion of dimethylfuran [11] or hydrodeoxygenation of fructose [12] to dimethyltetrahydrofuran (DMTHF). Besides, the larger size of the reactant and product may also highlight the role of the accessibility to the active sites of the catalysts in liquid media.

Among possible homogeneous or heterogeneous catalysts used for the diol cyclodehydrations, a layered material, $HNbMoO_6$, was found to catalyze the cyclization of 1,4-butanediol [2]. It also exhibited remarkable activity for several acid-catalyzed reactions, such as Friedel-Crafts alkylation, esterification, acetalization, condensation, hydration, and hydrolysis [2,13–18], notably the hydrolysis of saccharides [14] with the transformation of sucrose into glucose and fructose. More generally, in view of their stability and their tolerance to water, acidic layered materials could be promising candidates for catalysis in the liquid phase, notably in the context of biomass conversions. Among them, $HNbMoO_6$ could act as a representative layered catalyst.

Protonated layered transition metal oxides materials of the form $HNbMO_6$ (M = Mo, W) are trirutile-type crystalline structures made of MO_6 and NbO_6 octahedral slabs with H_3O^+ present in the interlayers [19–21]. This class of materials is remarkable due to the presence of a high density of strong acid sites within its interlayers [13,15,19,22] in addition to being water-tolerant [14,19]. Despite their quantity and strength, the interlayer acidic sites are generally not accessible by reactants due to the high charge density of the oxide sheets [13,23] thus rendering the catalyst non-active in its “as-prepared” form. Conversely, catalytic activity can be obtained if the reactant succeeds to intercalate within the interlayer. Interestingly, intercalation is now a method widely used to functionalize layered materials. Different approaches can be used to

favor and study the intercalation process, and several recent works have reviewed intercalation on various types of layered materials.[24–27] Some studies have notably investigated the possible intercalation of alcohols or diols in layered metal oxides.[28,29]

In the case of the $HNbMO_6$ solids, intercalation occurs via an acid-base reaction between the acidic sites available in the interlayers of the protonated layered materials and the upcoming basic substrates resulting in the expansion of the layers, thus allowing full accessibility to their acidic sites. We showed recently that the specific access to the acidic sites on such layered materials could be monitored by base intercalation followed by Raman spectroscopy [30], but this should be compared to catalytic results.

The successful cyclization of 1,4-butanediol or erythritol, two linear (non-branched) diols, to their corresponding 5-membered ring cyclic ether derivatives using $HNbMoO_6$ as a catalyst was attributed to their intercalation within $HNbMoO_6$ interlayers [2]. The same catalyst can be used for the hydrolysis of saccharides [14]. Transforming sucrose into glucose and fructose was attributed to the intercalation of the saccharide substrate into the interlayer gallery. Similarly, sorbitol could be dehydrated to 1,4-sorbitan due to the selective intercalation of sorbitol within $HNbMoO_6$ interlayers [31]. In this case, only hexane-1,6-diol and sorbitol could intercalate in the solid, as shown by the basal expansion observed by XRD after immersion, while the cyclodehydrated products, 1,4-sorbitan and isosorbide, were not able to induce any expansion of the layers. Takagaki et al. [16] further investigated the role of hydroxyl groups present in the organic substrates on the intercalation process and, consequently, the success of the reaction. Two molecules: lactic acid (a hydroxycarboxylic acid) and acetic acid were tested. While the esterification of acetic acid was nearly negligible, lactic acid encountered remarkable activity due to its intercalation (or protonic activation) within the interlayers of the solid catalyst. Moreover, successful esterification of acetic acid over $HNbMoO_6$ in the presence of lactic acid ensured the role of -OH groups on the intercalation process; the hydroxyl groups of lactic acid

induced an expansion of the interlayers allowing the accessibility of acetic acid to the active sites. For all the preceding examples, intercalation is manifested as the key feature for the resulting catalytic activity. This was evidenced by the rapid consumption of a starting material before the gradual formation of the desired product or by the increase of the interlayer spacing at the end of the reaction compared to its initial value. As accessibility to the active sites in liquid media is a key to develop new active catalysts, it would be interesting to follow the intercalation process and the evolution of the catalyst throughout the reaction. In addition, to evaluate the relative roles of acidity and accessibility to the active sites (intercalation) in liquid media, the availability of a simple catalytic test that can compare several (layered) catalysts would be desirable.

Therefore, in order to understand the influence of accessibility on the catalytic performance of layered materials, the present article aims to:

(i) Evaluate the potential of hexane-2,5-diol cyclodehydration into 2,5-dimethyltetrahydrofuran using mild reaction conditions in the liquid phase that can clearly distinguish between various solid acid catalysts, such as zeolites that can also show geometric constraints; (ii) Determine the influence of several reaction conditions, various temperatures and amounts of water, on the activity of a typical protonated layered transition metal oxide material, $HNbMoO_6$, without any pretreatment activation ; (iii) Compare the catalytic activity of $HNbMoO_6$ to those of other layered transition metal oxides $HNbWO_6$ and $H_2W_2O_7$; (iv) Emphasize the role of the intercalation process in the catalytic activity, notably by studying the intercalation process throughout the reaction by PXRD and Raman spectroscopy including the cyclization of diol by operando Raman spectroscopy.

2. Study of the hexane-2,5-diol cyclodehydration reaction

2.1. Cyclodehydration of pure hexane-2,5-diol

The activity of $HNbMoO_6$ towards the cyclodehydration of hexane-2,5-diol was first studied at 120 °C under solvent-free conditions (**Figure 1**, **Table 1**). A fast consumption of hexane-2,5-diol was noted from the very beginning of the reaction (15% after 5 minutes) and visually, an instant color change occurred on this solid from yellow to green within the first minutes; the conversion increased rapidly to reach 47% after 15 minutes and 95 % after 60 min. The strong conversion over $HNbMoO_6$ was associated with a high selectivity towards the formation of 2,5-dimethyltetrahydrofuran (DMTHF). Selectivities ranging between 88% and 94% were recorded even at high conversions. Conversely, a blank reaction without catalyst carried out by stirring hexane-2,5-diol at 120 °C yielded neither the desired product nor any by-product after 24 h of heating. Therefore, an acid catalyst is required for this reaction.

For comparison, the reaction was performed using some zeolite catalysts (Figure 1, Table 1). H-Y zeolite presented a weak conversion of about 17% after 30 minutes with no additional conversion after prolonged periods. A slightly higher but modest conversion was achieved, with ZSM-5 reaching 24 % in 60 min. On the other hand, H-beta zeolite showed a relatively better activity with 61% conversion after 60 min. The different tested catalysts follow the order $HNbMoO_6$ > H-Beta >> ZSM-5 > H-Y. All the active catalysts showed high selectivity following the order H-Beta (100 %) = H-Y (100 %) > $HNbMoO_6$ (95 %) > ZSM-5 (82%). Selectivities compared at ca. 20% conversion are reported in **Supporting information, Table S1**. Therefore, this test is able to discriminate between different solid catalysts. Additionally, it reveals that a layered catalyst, $HNbMoO_6$, can show a higher activity than conventional zeolite catalysts per catalyst weight, even though its surface area is initially quite low (Supplementary Information Table S2). Noteworthy, unlike the other tested catalysts which were used after a preliminary heat treatment, $HNbMoO_6$ could be used as-prepared i.e., without any pretreatment.

Besides, a leaching test showed that its catalytic activity was solely due to the solid itself (see Supplementary Information).

$HNbMoO_6$ giving the best performance in this reaction, it will be used subsequently to investigate the features of the cyclodehydration reaction.

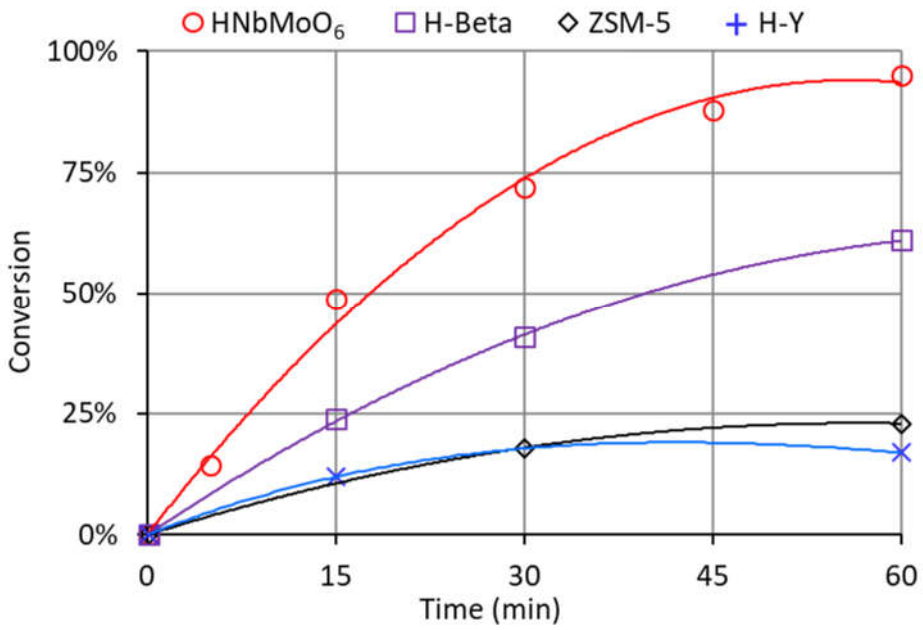

Figure 1. Conversion of hexane-2,5-diol as a function of elapsed time over different solid acid catalysts (T = 120 °C).

Table 1. Conversion of hexane-2,5-diol and selectivity towards the formation of 2,5-dimethyltetrahydrofuran using different solid catalysts at t = 60 min.

Catalyst	Conversion	Selectivity	Yield
$HNbMoO_6$	95%	95%	90%
[a]H-Beta	61%	100%	61%
[a]ZSM-5	23%	82%	19%
[a]H-Y	17%	100%	17%

Reaction conditions: m(hexane-2,5-diol) = 1 g, m(catalyst) = 55.6 mg, T = 120 °C, t = 60 min.
[a] Catalysts activated for 6 h at 450 °C.

2.2. Influence of temperature

The cyclodehydration of hexane-2,5-diol was tested at various temperatures. Expectedly, the conversion increases with the temperature (**Figure 2** and **Supporting information Figures S1-S4**). The time required to achieve 50 % conversion decreased from 520 min to 110 min, 18 min, and 10 min upon increasing the reaction temperature from 80 °C to 100 °C, 120 °C, and 140 °C, respectively (Supporting information Table S3). The selectivity towards 2,5-dimethyltetrahydrofuran remained high in all cases (85-95 %) even at high conversions.

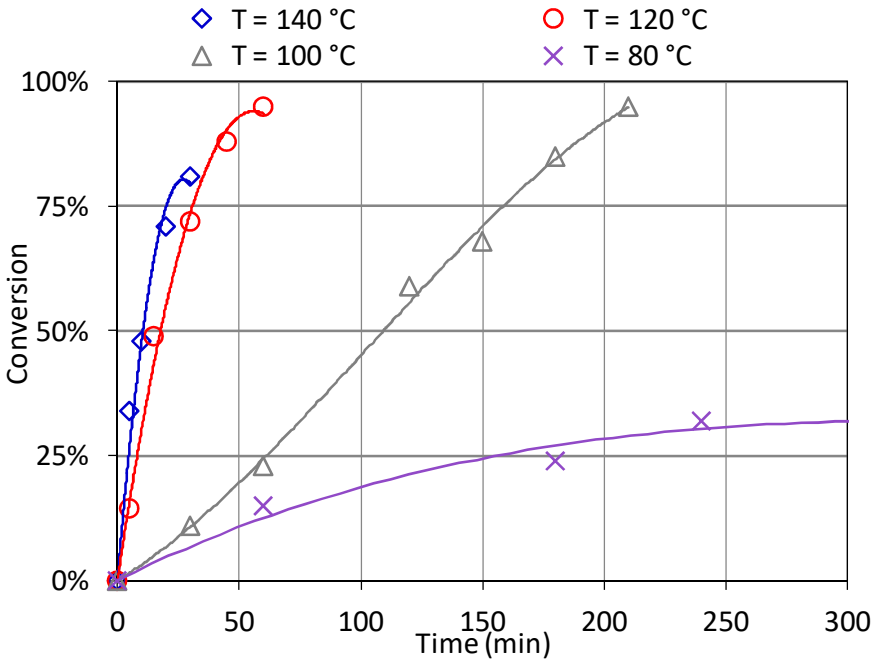

Figure 2. Conversion of hexane-2,5-diol as a function of elapsed time at different temperatures.

The activation energy for hexane-2,5-diol cyclodehydration over $HNbMoO_6$ was estimated from the Arrhenius plot and equal to 78.5 kJ mol^{-1} (Supporting information Figure S5).

2.3. Raman operando

The cyclization process was additionally monitored by operando Raman spectroscopy at 100 °C in the absence of solvent (**Figure 3**). Initially, only the bands due to hexane-2,5-diol were recorded. Upon heating, the intensity of the bands at 750, 820 and 860 cm^{-1} (denoted as red

triangles in Figure 3) decreased together with the growth of new bands at 805 and 880 cm^{-1} (denoted as green circles) corresponding to 2,5-DMTHF. This confirms the absence of any additional product. Deconvolution of the region 700-900 cm^{-1} revealed the appearance of the 805 cm^{-1} band after 30 min reaction (Figure S12). The relative amount of product in the reaction mixture was estimated by calculating the ratio of the band area at 800 to the sum of the bands at 800 and 820 cm^{-1} (Figure 3c). This calculation was made with the hypothesis of an equal Raman cross-section for the neighboring bands at 800 and 820 cm^{-1}. At t = 30 min, the ratio ($R_{800/(800+820)}$) increased sharply with time up to 90 minutes. At this instant, the band at 800 cm^{-1} became clear, as illustrated in Figure 3b. After this point, the ratio increased further but more slowly in line with the consumption of the major part of the starting material to become nearly stable after an additional 20 min. The product evolution under reaction monitored by Raman spectroscopy was overall consistent with the results obtained by gas chromatography.

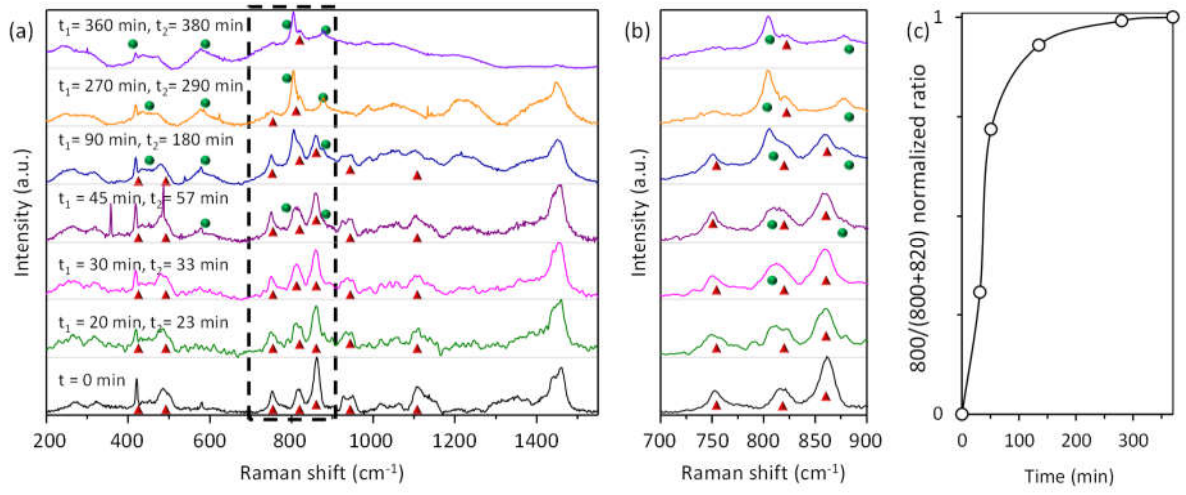

Figure 3. (a) Evolution of the Raman spectra of the reaction mixture upon heating at 100 °C in the absence of solvent. t_1 = beginning of the spectral recording, t_2 = end of the spectral recording, the stirring was stopped between t_1 and t_2. (b) Zoom in the region 700-900 cm^{-1}. Red triangles refer to bands of hexane-2,5-diol, green circles refer to bands of 2,5-dimethyltetrahydrofuran. (c) Ratio of the band intensities at 800/(800+820) cm^{-1} versus time at middle of spectral recording ($(t_1+t_2)/2$)).

2.4. Influence of dilution in water

To examine the influence of water on hexane-2,5-diol cyclodehydration, batches including H_2O/diol molar ratios of 1, 3, 10, and 98 were heated at 120 °C in the presence of $HNbMoO_6$. The increasing amounts of H_2O slowed down the reaction (**Figure 4** and Supporting information Figures S6-S9); this could be due to the competition on the active sites between water and the diol. For instance, the time required to achieve 50 % conversion was increased from 18 to 100, 350, 600, and 1400 minutes following the successive increase of H_2O/diol ratio from 0 to 1, 3, 10, and 98, respectively (Supporting information Table S4). The selectivity of the reaction is found to be in the range of 87 to 92 % for H_2O/diol ≤ 10. This result is similar to that obtained under solvent-free conditions; however, it drops to 59 % in the presence of a huge excess of H_2O (98 equivalents) where unidentified secondary products were formed. For H_2O/diol ≤ 10, the absence of change in selectivity and the progressive decrease of the conversion do not indicate any poisoning effect of water.

The formation of the 2,5-dimethyltetrahydrofuran is likely due to an SN2 nucleophilic substitution (see the reaction Schemes 1 and 2 shown in Supplementary Information).

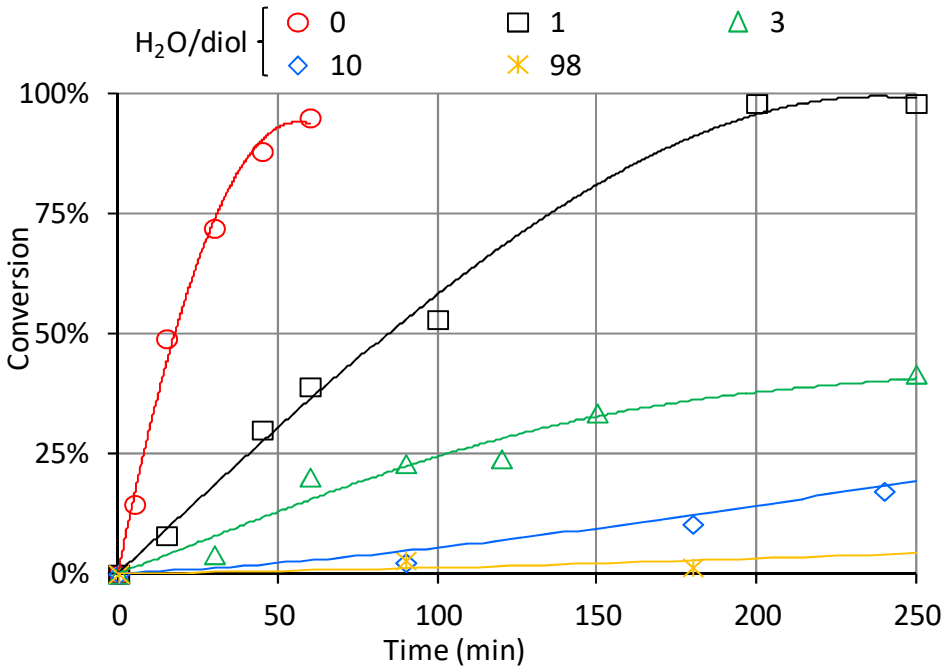

Figure 4. Conversion of hexane-2,5-diol as a function of elapsed time at different H_2O/diol ratios (T = 120 °C).

3. **Comparison of layered transition metal oxides ($HNbMoO_6$, $HNbWO_6$, and $H_2W_2O_7$)**

The above results show that layered $HNbMoO_6$ exhibits the highest catalytic activity among the various reference solid acid catalysts. It was thus compared with other layered oxides based on similar transition metals: $HNbWO_6$ and $H_2W_2O_7$. The structures of these solids were compared in our previous work.[30] $H_2W_2O_7$ is synthesized from $Bi_2W_2O_9$ which is related to the Aurivillius family of the layered perovskites constituted of bismuth oxide sheets and octahedral ReO_3^- like slabs. $H_2W_2O_7$ is then obtained from the precursor through selective acid leaching of $Bi_2O_2^{2+}$ sheets. $HNbWO_6$ structure is very close to that of $HNbMoO_6$, These layered solids had a very low surface area (<10 $m^2\ g^{-1}$, Table S2),[15,23,32] which confirms the bulk nature of the layered solids far below the large surfaces obtained when these solids are delaminated to nanosheets.[23] They were constituted by plate-like aggregates of 1-5 µm size (Supporting Information, Figure S10).

Their conversion in the catalytic transformation of hexane-2,5-diol was further examined. The reactions were carried out at 120 °C under solvent-free conditions (**Figure 5**).

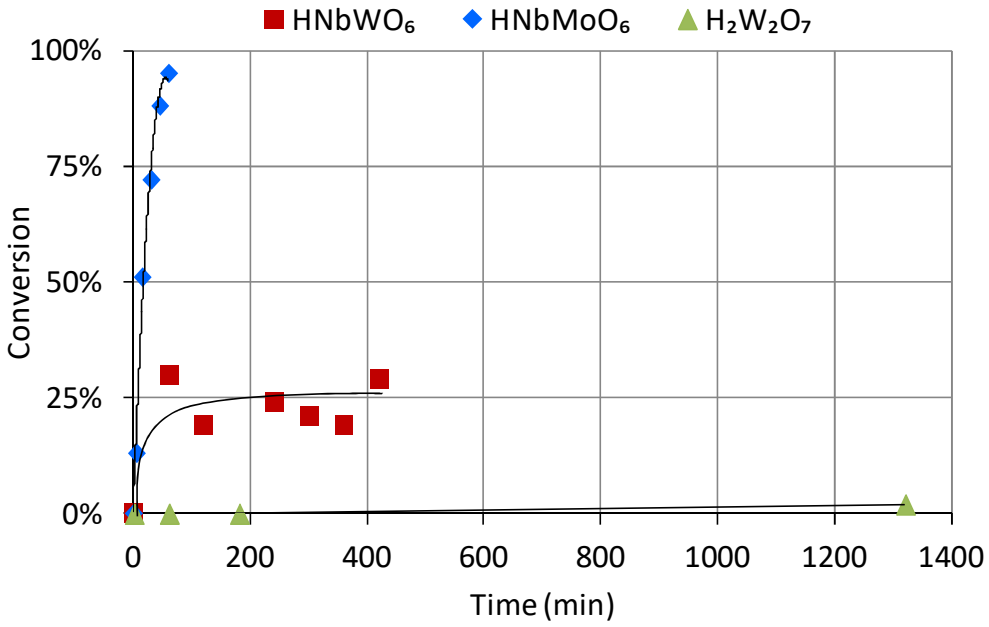

Figure 5. Conversion of hexane-2,5-diol at 120 °C as a function of elapsed time over $HNbMoO_6$, $HNbWO_6$, and $H_2W_2O_7$ layered catalysts.

Compared to the high conversion (95 %) and selectivity (95 %) exhibited by $HNbMoO_6$ after 1 h, $HNbWO_6$ demonstrated a low conversion of around 25 % after 7 hours with a very low selectivity (lower than 30 %). Meanwhile, no reaction took place over $H_2W_2O_7$; only 2 % conversion after 22 hours was calculated. One could wonder if $HNbWO_6$ could have been deactivated very quickly after a high initial conversion. However, heating at 150°C resulted in a higher conversion. The temperature used here is thus not sufficient for $HNbWO_6$ to compete with $HNbMoO_6$. Therefore, the order of activity of the catalyst for hexane-2,5-diol cyclodehydration can be represented as follows: $HNbMoO_6 >> HNbWO_6 \gg H_2W_2O_7$.

3.1. Role of the acidity

The activities measured for the different catalysts bring some indications on the kind of acidity required for the hexanediol cyclodehydration. Zeolites and $HNbMoO_6$ or $HNbWO_6$ [30], active in this reaction, all show principally Brønsted acidity. Nevertheless, activity and acidity are not clearly correlated. Although the zeolites have very different Si/Al ratios (ca. 40, 12.5, and 2.6 for ZSM-5, Beta, and HY respectively), they do not show a marked trend neither following the acid strength nor site density. Beta zeolite with an intermediate Si/Al ratio shows the largest activity of the three zeolites, while ZSM-5 (highest Si/Al) or HY (lowest Si/Al) show low and similar conversions.

To evaluate the acidity of the layered materials, adsorption of pyridine vapor was followed by FTIR spectroscopy (Supplementary Information, Figure S11 and Table S5). Similar to our previous results in the liquid phase followed by Raman spectroscopy [30], $H_2W_2O_7$ showed hardly any acidity, which explains the catalytic inactivity of this solid. In line with previous data[18,30,32], $HNbMoO_6$ and $HNbWO_6$ showed comparable acid features. Per mass unit, $HNbMoO_6$ showed more sites than $HNbWO_6$, but both solids were fully equivalent when referring to the surface density (Table S5). Nevertheless, the slight difference in the number of acid sites cannot account

for the conversion over $HNbMoO_6$ nearly 4 times higher than $HNbWO_6$, which is slightly more active than ZSM-5 or HY.

Therefore, although a minimum of Brønsted acidity is probably necessary to achieve the conversion of the hexanediol, as exemplified by the low conversion over the low Si/Al HY, acidity in itself is not sufficient to explain the results obtained. Interestingly, ZSM-5, with its smaller pore structure than Beta or HY, shows a lower selectivity to dimethylfuran, probably highlighting geometric constraints on the formation of the cyclic furan. Nevertheless, despite the large difference in surface area between zeolites and the layered solids, $HNbMoO_6$ shows a high activity. Besides, it is noteworthy that a much lower selectivity is also observed for $HNbWO_6$. Accessibility and steric constraints may thus have a major impact on this reaction. Interestingly, in the esterification of acetic acid with butanol, the lower conversion over $HNbWO_6$ compared to $HNbMoO_6$ was attributed to the higher gallery height of $HNbMoO_6$ [18]. Accessibility and intercalation will thus be studied in the next section focusing only on the layered materials (zeolites geometric selectivity is indeed well known, and several reliable test reactions are already well-documented for zeolites).

3.2. Intercalation

The catalytic activity of $HNbMoO_6$ is often attributed to the successful intercalation of the substrates within its interlayers;[2,13–16,31] however, intercalation was not studied in the course of the reactions. In our case, evidence of intercalation was noted from the very beginning of the reaction. PXRD patterns were monitored to follow the evolution of the intercalation process (**Figure 6** and **Table 2**). In any case, the reflection (110) at 26.8° was not modified, demonstrating the preservation of the in-plane catalyst structure. By contrast, the (001) reflection largely varied, highlighting the expansion of the interlayer spacing. This peak evolved

from 6.38° to 5.59° (Figure 6A) after 5 minutes from heating at 120 °C under solvent-free conditions, indicating fast intercalation of the diol within the interlayer of $HNbMoO_6$. A low intense peak was still present at 6.38° revealing that the active sites were not fully occupied by hexane-2,5-diol at that time leaving part of the interlayer distance unmodified; nevertheless, at 5 min, 15 % of hexane-2,5-diol has already been converted to 2,5-DMTHF thus illustrating the rapidity and efficiency of the active sites in promoting the cyclization subsequently after intercalation. At t = 15 minutes, the distribution of hexane-2,5-diol inside the layers becomes more homogeneous, evidenced by the presence of one single peak at 6.10° with an interlayer distance of 1.48 nm (Table 2). For longer reaction periods, a further successive decrease of the position of the (001) peak is recorded; deconvolution of these basal spacing peaks revealed the presence of a second peak (phase 2) indicative of a different filling of the interlayer, with interlayer spacing ranging between 1.58 nm and 1.62 nm larger than that recorded at $t \leq 15$ min. The population of this phase is found to increase with time, reaching 90 % at t = 60 min (Figure S13). These interlayer spacings are consistent with those obtained in the case of butane-1,4-diol [2] or sorbitol and somewhat larger than for hexane-1,6-diol (1.5 nm) [31]. Similar geometries are probably involved with these various compounds. These data also demonstrate the importance of the intercalation process on the catalytic reaction. It occurs instantly, allowing the diffusion of the diol into the interlayer acidic sites and, consequently, the rapid formation of the desired product. Additionally, intercalation appears as a dynamic process; the progressive uptake of diol results in an additional increase of the interlayer spacing and even induces the presence of an additional phase with larger interlayer spacing. However, this may occur in a non-homogeneous way, which explains some irregularities in the evolution of the peaks at the early stages of the reaction.

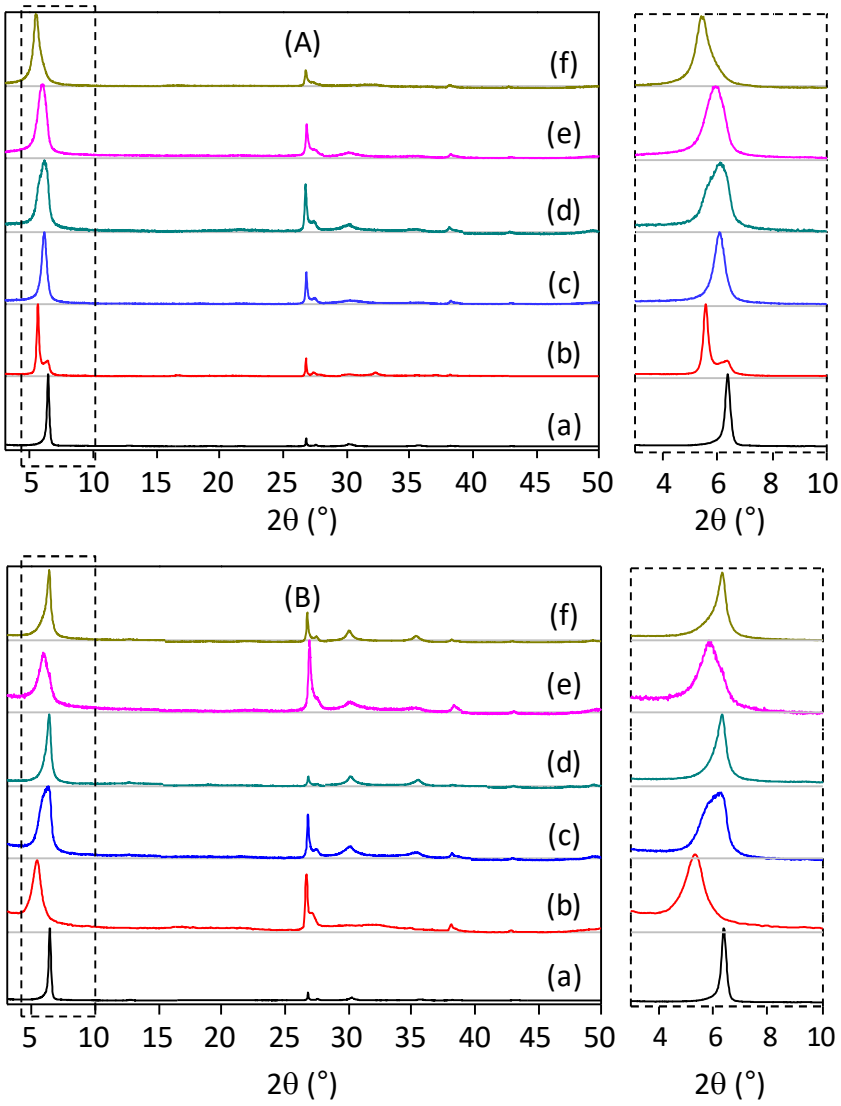

Figure 6. Evolution of PXRD pattern of $HNbMoO_6$ during cyclization of hexane-2,5-diol at 120 °C . (A) Under solvent-free conditions : (a) hydrated, (b) at t=5 min, (c) 15 min, (d) 30 min, (e) 45 min, and (f) 60 min. (B) After dilution in water : (a) untreated $HNbMoO_6$ and $HNbMoO_6$ collected at the end of reaction with diol/H_2O molar ratio of (b) 1:0, (c) 1:1, (d) 1:3, (e) 1:10, and (f) 1:98.

In the presence of water, the in-plane crystal structure (110) remained unchanged in all the PXRD patterns reflecting the stability of $HNbMoO_6$ towards water while the position of the (001) reflection moved towards higher d values. The successive increase in H_2O content resulted in a progressive shift of the (001) peak from 5.63° (diol:H_2O 1:0) up to 5.93° (diol:H_2O 1:1), 6.33° (diol:H_2O 1:3), 5.90° (diol:H_2O 1:10), and 6.26° (diol:H_2O 1:98) corresponding to a decrease of the d-interlayer spacing (Figure 6B). Consequently, a lower expansion of the

layers was observed for phases 1 and 2 (Table 2). Increasing amounts of H_2O are thus filling the interlayers, which may decrease the number of active sites accessible by the diol and explain the longer contact time required to achieve a good conversion.

The difference in the catalytic activity between $HNbMoO_6$ and the two other layered transition metal oxides ($HNbWO_6$ and $H_2W_2O_7$) was studied using the powder X-ray diffraction results (**Figure 7**). Due to their lower conversion, $HNbWO_6$ and $H_2W_2O_7$ powders were collected only at the end of the reaction.

Table 2. Evolution of lattice parameters of $HNbMoO_6$ catalyst at various reaction conditions (T = 120 °C).

Diol:H_2O[a]	**Time (min)**	**d-interlayer (Å)**			**Main peak $2\theta_{(001)}$ (°)**
		Phase 0	Phase 1	Phase 2	
	hydrated	13.843			6.379
1:0	15		14.86(2)		6.098
1:0	30		14.50(3)	15.75(6)	5.900
1:0	45		14.76(3)	15.75(5)	5.953
1:0	60		14.73(7)	16.19(2)	5.631
1:0	150			16.45(6)	5.448
1:1	150		14.52(3)	15.92(5)	5.935
1:3	400		14.16(3)	15.71(4)	6.333
1:10	1740		14.94(3)	16.44(8)	5.904
1:98	360		14.26(1)		6.289
1:98	3120		14.11(2)	15.41(3)	6.262

[a]molar ratio before reaction.

While the (001) diffraction peak of $HNbMoO_6$ shifted from 6.38° to 5.63° after 60 minutes of reaction, $HNbWO_6$ only encountered a very slight shift in the (001) diffraction peak from 7 to 6.94° after 24 hours. This shift in the peak highlights the much lower intercalation occurring in $HNbWO_6$ than in $HNbMoO_6$. This could be attributed to the smaller gallery height of $HNbWO_6$ (0.496 nm) than that of $HNbMoO_6$ (0.553 nm) [18]. Consequently, the intercalation of hexane-

2,5-diol into the interlayer gallery of layered $HNbWO_6$ is more difficult, resulting in a lower conversion.

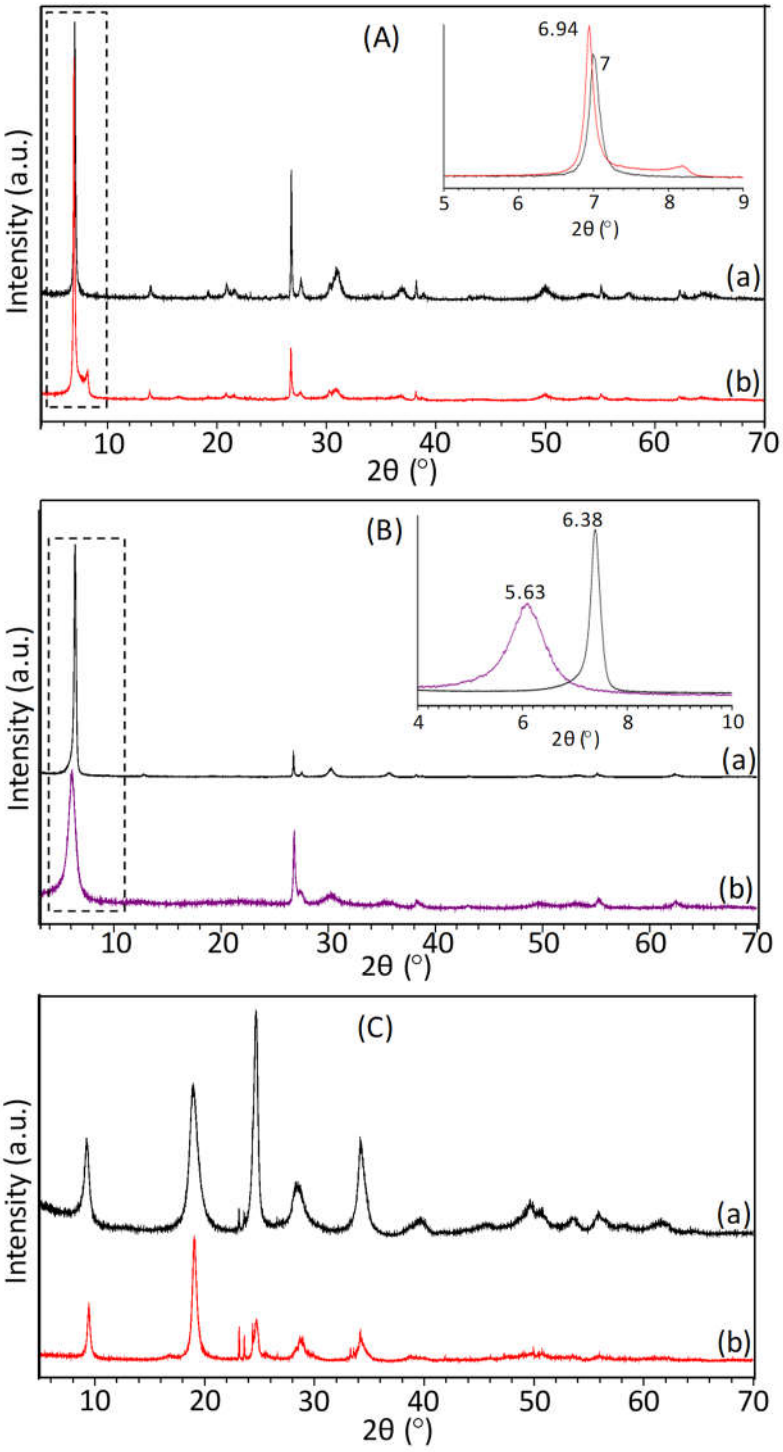

Figure 7. PXRD patterns of (A) $HNbWO_6$, (B) $HNbMoO_6$ and (C) $H_2W_2O_7$ at (a) hydrated and (b) after reaction (time=60 min in (B) and 24 h in (A) and (C)). The insets in (A) and (B) show the enlargement below 10°.

In the case of $H_2W_2O_7$ layered oxide, PXRD patterns did not show any significant change, except for the decrease in intensity at 25°, revealing that no intercalation or interaction occurred. The protons are too weak or too scarce to promote any catalytic conversion. This is also consistent with the absence of intercalation of pyridine in its structure [30].

Therefore, our results emphasize that intercalation is a key factor to permit the successful catalytic reaction over layered metal oxides, and the cyclodehydration of hexane-2,5-diol can discriminate layered solids based on their intercalation ability.

3.3. Raman study of the catalyst stability

Finally, the evolution and stability of the catalyst were also evaluated throughout the reaction by Raman spectroscopy **(Figure 8)**. Powders collected at different instants of the reaction, both in the absence and in the presence of various amounts of H_2O at 120 °C revealed similar profiles without the disappearance of any $HNbMoO_6$ bands or major formation of new ones, which illustrates the stability of the catalyst in agreement with the results from PXRD analyses. Yet, the different bands were not affected in the same manner (Table S6 and Figure S14). During reaction in the absence of water, bands solely related to Molybdenum species (υ(Mo=O) at ca. 974 cm^{-1} and υ(Mo-O-Mo) at 818 cm^{-1}) shifted moderately, until conversion was ~70%. By contrast, bands involving Niobium (υ(Nb=O) at 903 cm^{-1} and υ(O-Nb-O) at 461 cm^{-1}) encountered an important, progressive displacement throughout the reaction reaching -23 cm^{-1} and -9 cm^{-1}, respectively until 45 min (88 % conversion) before shifting back due to the lower quantity of hexane-2,5-diol available for intercalation and cyclization. The mixed υ(Nb-O-Mo) at 604 cm^{-1} encountered an intermediate shift of -13 cm^{-1}, at 15 min (49% conversion) before shifting back for higher times and conversions. A broad band is also observed at around 730 cm^{-1}. Similar trends were noticed in the presence of water at 120°C, although soaking $HNbMoO_6$ in water at room temperature did not induce any additional change in the Raman profile (Figure 8B-b). After reaction at 120 °C in the presence of water, υ(Mo=O) and υ(Mo-

O-Mo) exhibit minor deviation. Meanwhile, υ(Nb=O) constantly shifted with increasing water contents reaching -29 cm^{-1} at Diol:H_2O, 1:98. Therefore, if Molybdenum sites seem to be important in the vicinity of the reaction sites, Nb-O-Mo sites are probably the most affected in the initial steps of the reaction, notably during the intercalation. The milder Nb=O sites that can adsorb hexanediol are also very sensitive to the perturbations by water (as a reaction product or solvent).

Like PXRD, Raman indicates the significant influence of the reaction mixture on the catalyst. Intercalation occurs readily in the initial stages of the reaction, which enables favored interactions between the diol or water with the surface of the inorganic slabs.

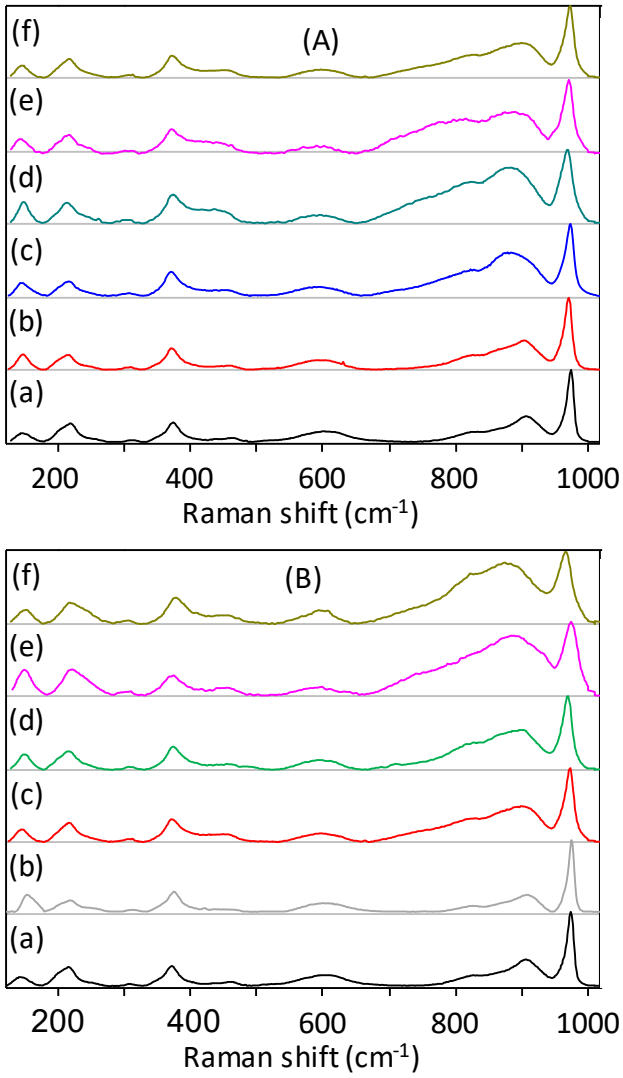

Figure 8. (A) Evolution of the Raman shift of $HNbMoO_6$ during cyclization of hexane-2,5-diol at 120 °C, t = (a) 0 min, (b) 5min, (c) 15 min, (d) 30 min, (e) 45 min, and (f) 150 min (T = 120 °C). (B) Raman profiles of $HNbMoO_6$ untreated (a), mixed with 1 mL of H_2O (diol/H_2O = 0) at T = 25 °C (b), and $HNbMoO_6$ collected at the end of reaction (T = 120 °C) with diol/H_2O molar ratio of (c) 1:0, (d) 1:3, (e) 1:10, and (f) 1:98.

The interaction of hexane-2,5-diol with $HNbWO_6$ and $H_2W_2O_7$ was also monitored by Raman spectroscopy. The powder samples collected at the end of the reaction were dried, characterized by Raman spectroscopy, and compared with their initial ones (**Figure 9**).

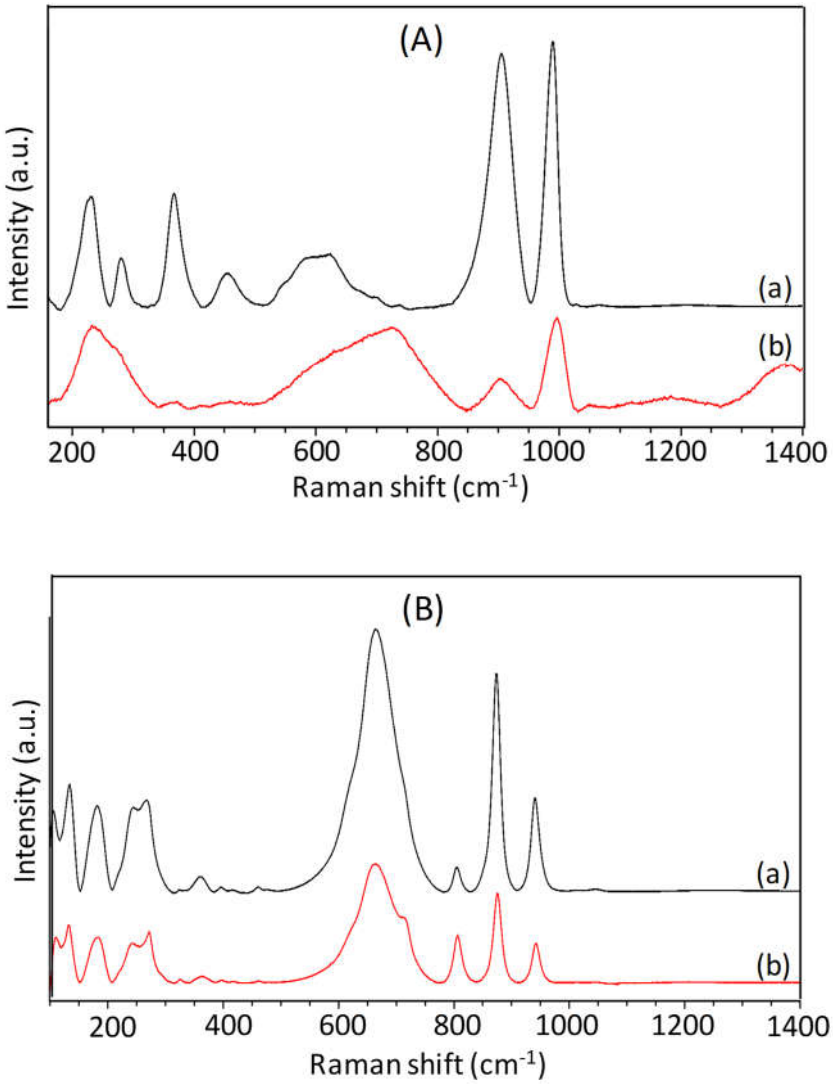

Figure 9. Raman spectra of (A) $HNbWO_6$ and (B) $H_2W_2O_7$ before reaction (a) and after 24 hours reaction at 120 °C (b).

After the reaction, the Raman profile of $H_2W_2O_7$ layered oxide remained intact, indicating the absence of interaction with hexane-2,5-diol in agreement with the results obtained from the catalytic test and PXRD studies. A contrast behavior was observed for $HNbWO_6$. The Raman shifts of ν(W=O) and ν(Nb=O) did not change, yet the ν(Nb=O) band broadened and strongly decreased in intensity while a new band appeared at 723 cm^{-1} that can be due to the interaction between the Nb=O sites and the product perturbating also the υ(Nb-O-W) band around 613 cm^{-1}. Compared to $HNbMoO_6$, these observations indicate a partial interaction with the surface maybe limited to the most external sites but like for $HNbMoO_6$, niobate and Nb-O-W sites are likely to play a predominant role in the interactions with hexanediol.

4. Conclusions

Several layered materials based on transition metals were evaluated as potential heterogeneous catalysts. The cyclodehydration of hexane-2,5-diol into 2,5-dimethyltetrahydrofuran can be used as a model reaction to characterize solid acid layered catalysts in the liquid phase at medium temperature. This test could be helpful in the selection of catalysts for some biomass conversions. In particular, this reaction highlights the accessibility to the active sites of layered materials in liquids.

The layered $HNbMoO_6$, used as a catalyst for this reaction, outperformed more conventional catalysts such as zeolites and other transition metals-based layered catalysts ($HNbWO_6$ and $H_2W_2O_7$). The reaction was also carried out in the presence of water, where $HNbMoO_6$ showed a high water tolerance.

Activity on layered materials is attributed to both the presence of Brønsted acidity and the capacity to intercalate the hexanediol reactant. $H_2W_2O_7$ proved to be unable to intercalate base molecules and was completely inactive. By contrast, although $HNbWO_6$ is similar to $HNbMoO_6$ both in structure and acidity, it was far less active. By monitoring intercalation using PXRD

and Raman spectroscopy, the difference in catalytic activity and selectivity appears directly related to the ability to intercalate the diol reactant.

Finally, Raman spectroscopy of the active $HNbMoO_6$ catalyst in the presence of hexanediol or water suggests that sites related to niobium could act more preferentially as adsorption/intercalation sites compared to pure molybdates/tungstates.

5. Experimental Section

5.1. Materials: Hexane-2,5-diol was purchased from Fluorochem (Derbyshire, UK), ZSM-5 (H-90, Si/Al = 40-45), Zeolite Beta (BEA, CP B/4E Si/Al = 12.5) and Zeolite Y (NH_4-Y, Si/Al = 2.6) were purchased from Zeolyst. The H-form of zeolite Y (H-Y) was prepared by calcining the ammonium form at 550 °C for 6h with a ramp of 1.5 °C/min, under static air.

Layered $HNbMoO_6$, $HNbWO_6$ and $H_2W_2O_7$ were prepared by proton-exchange of the precursors $LiNbMoO_6$, $LiNbWO_6$ and $Bi_2W_2O_9$ respectively. The synthesis details are reported in reference [30]. The complete protonation was ensured following the PXRD pattern that matches the PXRD patterns reported in the literature[30].

5.2. Catalytic conversion of hexane-2,5-diol into 2,5-dimethyltetrahydrofuran

a) Reaction general conditions: $HNbMoO_6$ was used without any further treatment or preliminary activation step. For 1 g (8.46 mmol) of hexane-2,5-diol, 55.6 mg of $HNbMoO_6$ were stirred at 80, 100, 120, or 140 °C for various time intervals (5 min-1440 min). For all reactions, a cooler was placed on top of the reactor, in reflux-like conditions, to ascertain that the dimethyl tetrahydrofuran product (b.p.=93°C) or water were not evaporated in the course of the reaction.

b) Tests with other catalysts: 55.6 mg of catalysts were stirred with 1 g (8.46 mmol) of hexane-2,5-diol under reflux at 120 °C for 15-60 min (H-ZSM-5, H-Beta and H-Y), 440 min

($HNbWO_6$), or 1350 min ($H_2W_2O_7$). $HNbWO_6$ and $H_2W_2O_7$ were not activated prior to use. The zeolites were activated at 450 °C for 6 h under a flow of dry air of 20 ml/min. The activated samples were transported in closed reactors and introduced into the reaction container under argon flow.

c) Influence of water: the influence of various amounts of water on the reaction features was studied by introducing, for 1 g of hexane-2,5-diol and 55.6 mg of catalyst, either 152 mg of H_2O (8.44 mmol, 1 equivalent compared to the diol), 457 mg (25.39 mmol, 3 equivalents), 1.523 g (84.62 mmol, 10 equivalents), or 14.920 g (828.88 mmol, 98 equivalents). Reactions were then carried out at 120 °C for 30 min to 4080 min.

d) Catalytic test analyses in the liquid phase:

Gas chromatography: The conversion of hexane-2,5-diol was monitored by gas chromatography (GC) using Varian 3900 gas chromatograph equipped with FID detector and HP plot/Q column. The samples from the solvent-free reaction were prepared from 15 µL of the reaction mixture (readily passed over a microfilter to eliminate solid particles), 500 µL of dichloromethane, and 5 µL of 1-hexanol used as a standard. When the reaction was performed in the presence of water, to avoid problems of miscibility and over-dilution of the products to analyze, the samples were prepared with 18 µL of the reaction mixture (readily passed over a microfilter to eliminate solid particles), 100 µL of H_2O, and 5 µL of 1-propanol used as a standard.

Operando Raman spectroscopy: The catalytic transformation of hexane-2,5-diol into 2,5-dimethyltetrahydrofuran was monitored by Raman spectroscopy throughout the reaction in the absence of solvent at T = 100 °C. A green laser with 532 nm wavelength was used for excitation and a Raman probe (InPhotonics) lined to the spectrometer (Horiba Jobin Yvon Labram 300) via optical fibers was immersed into the liquid phase of the mixture. For longer

reaction times, the spectra were less resolved and required longer scanning periods. Therefore, the last points should rather be considered as the average data over the acquisition time.

e) Analyses of the solids: The powders collected at different reaction conditions were washed by dichloromethane to remove the reactant and products and then dried overnight at room temperature prior to structural analyses.

Powder X-ray diffraction (PXRD): powder samples were studied with *PANalytical* X'Pert Pro diffractometer using a CuKα monochromatized radiation (λ = 1.5418 Å). The PXRD patterns were analyzed using Jana 2006 program, then refined using whole powder pattern decomposition methods (also referred as Pawley [33] or Le Bail [34] methods).

Raman spectroscopy: Raman measurements on the solid catalysts were conducted on a Jobin Yvon Labram 300 confocal microscope. The confocal spectrometer was equipped with a 532 nm laser and a 1800 lines/mm grating. Laser power on the solid sample was ca. 5 mW, acquisition time varied from 2 min to 90 min.

Supporting Information

Supporting Information is available from the Wiley Online Library or from the author.

Acknowledgements

The authors acknowledge the financial support from the French Ministry of Education and Research and from the French Agence Nationale de la Recherche and LabEx EMC3 through the project OXYLAC (Grant No. ANR-10-LABX-09-01). The authors thank Sylvie Collin for her help in preparing the samples.

Conflict of Interest

The authors declare no conflict of interest.

Author Information

Corresponding Author

E-mail: guillaume.clet@ensicaen.fr

Present address

Moussa Zaarour's present address is:

King Abdullah University of Science and Technology, KAUST Catalysis Center (KCC), Catalysis Nanomaterials and Spectroscopy (CNS), Thuwal 23955, Saudi Arabia

References

[1] R. Rinaldi, F. Schüth, *Energy Environ. Sci.* **2009**, *2*, 610–626.
[2] A. Takagaki, *Catal. Sci. Technol.* **2016**, *6*, 791–799.
[3] A. Yamaguchi, N. Hiyoshi, O. Sato, M. Shirai, *ACS Catal.* **2011**, *1*, 67–69.
[4] S. M. Patel, U. V. Chudasama, P. A. Ganeshpure, *React. Kinet. Catal. Lett.* **2002**, *76*, 317–325.
[5] H. Li, H. Yin, T. Jiang, T. Hu, J. Wu, Y. Wada, *Catal. Commun.* **2006**, *7*, 778–782.
[6] B. Török, I. Bucsi, T. Beregszászi, I. Kapocsi, Á. Molnár, *J. Mol. Catal. Chem.* **1996**, *107*, 305–311.
[7] Á. Molnár, K. Felföldi, M. Bartók, *tetrahedron* **1981**, *37*, 2149–2151.
[8] A. Yamaguchi, N. Hiyoshi, O. Sato, M. Shirai, *ACS Catal.* **2011**, *1*, 67–69.
[9] M. -J. Kim, I. -S. Lee, *J Org Chem* **1993**, *58*, 6483–6485.
[10] M. Lj. Mihailovic, S. Gojkovic, Z. Cekovic, *J Chem Soc Perkin Trans 1* **1972**, *0*, 1–5.
[11] R. J. Sullivan, E. Latifi, B. K.-M. Chung, D. V. Soldatov, M. Schlaf, *ACS Catal.* **2014**, *4*, 4116–4128.
[12] M. A. Jackson, M. Appell, J. A. Blackburn, *Ind. Eng. Chem. Res.* **2015**, *54*, 7059–7066.
[13] C. Tagusagawa, A. Takagaki, S. Hayashi, K. Domen, *J. Am. Chem. Soc.* **2008**, *130*, 7230–7231.
[14] A. Takagaki, C. Tagusagawa, K. Domen, *Chem. Commun.* **2008**, *0*, 5363–5365.
[15] C. Tagusagawa, A. Takagaki, K. Takanabe, K. Ebitani, S. Hayashi, K. Domen, *J. Phys. Chem. C* **2009**, *113*, 17421–17427.
[16] A. Takagaki, R. Sasaki, C. Tagusagawa, K. Domen, *Top. Catal.* **2009**, *52*, 592–596.
[17] A. Takagaki, C. Tagusagawa, S. Hayashi, M. Hara, K. Domen, *Energy Env. Sci* **2010**, *3*, 82–93.
[18] J. He, Q. J. Li, Y. Tang, P. Yang, A. Li, R. Li, H. Z. Li, *Appl. Catal. Gen.* **2012**, *443–444*, 145–152.
[19] P. Shen, H. T. Zhang, H. Liu, J. Y. Xin, L. F. Fei, X. G. Luo, R. Z. Ma, S. J. Zhang, *J Mater Chem A* **2015**, *3*, 3456–3464.
[20] H. J. Nam, H. Kim, S. H. Chang, S. G. Kang, S. H. Byeon, *Solid State Ion.* **1999**, *120*, 189–195.
[21] N. S. P. Bhuvanesh, J. Gopalakrishnan, *Inorg. Chem.* **1995**, *34*, 3760–3764.
[22] C. Tagusagawa, A. Takagaki, S. Hayashi, K. Domen, *Catal. Today* **2009**, *142*, 267–271.
[23] C. Tagusagawa, A. Takagaki, S. Hayashi, K. Domen, *J. Phys. Chem. C* **2009**, *113*, 7831–7837.
[24] J. Zhou, Z. Lin, H. Ren, X. Duan, I. Shakir, Y. Huang, X. Duan, *Adv. Mater.* **2021**, *33*, 2004557.
[25] R. Uppuluri, A. Sen Gupta, A. S. Rosas, T. E. Mallouk, *Chem Soc Rev* **2018**, *47*, 2401–2430.
[26] A. Bashir, S. Ahad, L. A. Malik, A. Qureashi, T. Manzoor, G. N. Dar, A. H. Pandith, *Ind. Eng. Chem. Res.* **2020**, *59*, 22353–22397.
[27] X. Wang, W. Wei, J. Hu, S. Li, Y. Wang, L. Yin, X. Kong, Q. Feng, *Chem Commun* **2021**, *57*, 7394–7397.
[28] C. I. Thomas, M. Karppinen, *Inorg. Chem.* **2017**, *56*, 9132–9138.
[29] Y. Wang, M. Nikolopoulou, E. Delahaye, C. Leuvrey, F. Leroux, P. Rabu, G. Rogez, *Chem Sci* **2018**, *9*, 7104–7114.
[30] G. Fayad, P. Boullay, G. Clet, *J. Colloid Interface Sci.* **2020**, *570*, 41–51.
[31] Y. Morita, S. Furusato, A. Takagaki, S. Hayashi, R. Kikuchi, S. T. Oyama, *ChemSusChem* **2014**, *7*, 748–752.

[32] J. Zhong, Y. Guo, J. Chen, *J. Energy Chem.* **2017**, *26*, 147–154.
[33] G. S. Pawley, *J Appl Cryst* **1981**, *14*, 357–361.
[34] A. Le Bail, H. Duroy, J. L. Fourquet, *Mat Res Bull* **1988**, *23*, 447–452.